Materials Today: Proceedings xxx (xxxx) xxx

Contents lists available at ScienceDirect

Materials Today: Proceedings

journal homepage: www.elsevier.com/locate/matpr

Damage assessment of complete, filled fiberboard boxes in regulative vertical impact tests by dropping

Nikolaos Lengas [a,*], Sergej Johann [a], Daniel Kadoke [a], Karsten Müller [a], Eva Schlick-Hasper [a], Marcel Neitsch [a], Manfred W. Zehn [b]

[a] BAM Federal Institute for Materials Research and Testing, Unter den Eichen 87, 12205 Berlin, Germany
[b] TU Berlin, Institute of Mechanics, Straße des 17. Juni 135, 10623 Berlin, Germany

ARTICLE INFO

Article history:
Available online xxxx

Keywords:
Finite-element-method
Digital image correlation
Dangerous goods packagings
Corrugated fiberboard box
Drop test

ABSTRACT

Due to the high damping mechanical properties of fiberboard materials, corrugated fiberboard boxes are widely used as transport packagings of dangerous goods. Since there is risk of vertical impact within the distribution system, drop tests are performed as design type tests to assess a package's ability to withstand damage. In this context, however, little is known regarding the transient mechanical response of a filled fiberboard box. The reason is that the nature of the packaging material presents challenges in identifying the deformation mechanisms experimentally. The aim of this work is to provide a framework for predicting the damage resistance of complete, filled corrugated fiberboard boxes which are ready for transportation. Therein, drop test finite-element simulations are used and validated by experimental results. These numerical calculation models are a valuable tool for virtual product development and contribute to the optimization of the design cycle.

1. Introduction

Corrugated fiberboard boxes are an established type of dangerous goods packaging for transporting various hazardous substances. Therefore, certain requirements need to be met to ensure a uniform level of safety. These requirements are described in the United Nations Model Regulations [1] as well as in the Agreement concerning the International Carriage of Dangerous Goods by Road (ADR) [2]. Thus, to be approved, a packaging must pass design type tests, such as the drop test. Thereby, a complete, filled transport packaging shall be allowed to fall under gravity and get decelerated onto an impact target with an essentially unyielding surface [3]. The purpose of the drop test is to assess a package's resistance to mechanical damage since vertical impact can occur in the transportation chain.

A main requirement for drop tests of dangerous goods packagings, as referred to in ISO 2248 [3], is that the impact surface shall be integral with a mass at least 50 times that of the heaviest package to be tested. However, manufacturers of corrugated fiberboard boxes often do not have an appropriate testing device to meet this requirement, signifying that they must outsource drop testing. Safety in transport is compromised if a packaging doesn't pass the drop test. This creates problems for manufacturers. Numerical simulations of a drop test can be a powerful assistance tool in the design process and ensure that the positions of critical loading of a filled box are identified correctly. Using this type of virtual product development, optimization of packaging design can occur before series production; hence, minimizing costs and maximizing performance.

This work addresses a deformation analysis of filled corrugated fiberboard boxes in the context of the mechanical safety testing of dangerous goods packagings. A finite-element (FE) model of the drop test is introduced that realistically describes the complex mechanical behavior of the packaging during impact. The model is validated experimentally using the digital image correlation (DIC) technique. DIC enables highly accurate measurements of deformations and strains on the fiberboard material, as well as vibrations of the impact surface. Additionally, accelerometers are applied on the impact surface as a redundant measurement of vibration data. Furthermore, the proposed drop test simulation model can be parametrized and used in sensitivity analyses. This

* Corresponding author.
E-mail address: nikolaos.lengas@bam.de (N. Lengas).

https://doi.org/10.1016/j.matpr.2023.04.679
2214-7853/

aims to determine failure mechanisms and bearable loads of different designs of filled corrugated fiberboard packagings within the scope of the transportation of dangerous goods.

2. Materials and methods

The test setup [4] comprises model impact target and filled corrugated fiberboard box. The model impact target consists of a steel plate with a mass ratio of 1:50 to the considered filled boxes which rests on a bedding of high strength spring elements. The corrugated fiberboard box design type complies with dangerous goods regulations [1,2] and is coded as 4G according to ADR 6.1.2.7 [2]. A polymethylmethacrylate (PMMA) granulate is used as a substitute filling substance and constitutes a homogeneous filling that causes great strains on impact. The combined weight of package and filling is 18 kg.

The defined loading scenario consists of a free drop of the filled fiberboard box onto the impact target's surface from predetermined critical heights. These drop heights diverge from the ones in ADR 6.1.5.3.5 [2] for drop testing of dangerous goods packagings. They have the purpose, however, to statistically determine the amount of impact energy needed so that the tested package has a 50 % probability to fail the drop test [5]. Failure of a drop test is defined as evident leakage of the filling substance. Thus, it is possible to identify the activated mechanisms of mechanical damage of the 4G packaging. Furthermore, the drop position according to ISO 2206 [6] is on the corner of the package to consider the worst-case impact loading.

The impact data were captured with the help of two high speed cameras by means of 3D deformation measurement and point tracking [7–9], as well as with Integrated Electronics Piezo-Electric (IEPE) accelerometers on the impact surface. The numerical analysis of the impact was developed by the commercially available simulation software LS-DYNA. This includes structural and material modeling in preprocessing (LS-PrePost), the FE solver (LS-DYNA), and postprocessing of the results (LS-PrePost).

2.1. Experimental setup of the drop test

The surface of a 980 kg steel plate is used as an impact target. Hence, the regulation requirement of a mass ratio of at least 1:50 between target and package is satisfied. For the purpose of controlling and minimizing the energy that gets transmitted outwards from the system and into the ground during impact, a set of five high strength spring elements is used as a bedding for the steel plate. The technical data of the model impact target are depicted in Fig. 1.

This impact target foundation structure has been verified to conform to regulations [2,3] and its properties are described in detail in the investigations regarding impact target requirements in the mechanical safety testing of dangerous goods packagings by Lengas et al [4].

The walls of the 4G packaging consist of a double faced and double-walled corrugated fiberboard in BC-profile. Its geometry is displayed in Fig. 2.

The values for the geometrical properties depicted in Fig. 2 are given in Table 1. The total wall thickness amounts to 6.72 mm and was measured as described in ISO 3034 [10].

The grammage values of the board composition are 125 g/m^2 for the top and bottom liner, 115 g/m^2 for the insert liner, and 150 g/m^2 for the B- and C-flute respectively. The corrugated fiberboard box geometry is designed as per drawing shown in Fig. 3 according to FEFCO 0201 [11].

The 40 mm wide gluing flap (manufacturer's joint) has been glued and taped at the outside of the outer packaging for the purpose of holding the two ends of the box blank together. Information regarding the dimensions of the entire empty packaging can be found in Table 2.

The substitute filling substance is a PMMA granulate with the commercial name Esplas H130. The substance's specifications can be found in [4]. It exhibits good flow properties in order to cause large strains in the fiberboard walls of the 4G box on impact, and homogeneity in its grain shape and size to increase test repro-

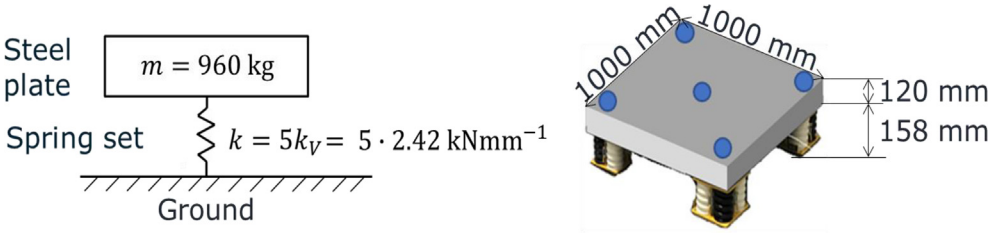

Fig. 1. Steel plate on spring element bedding as impact target foundation for the drop test.

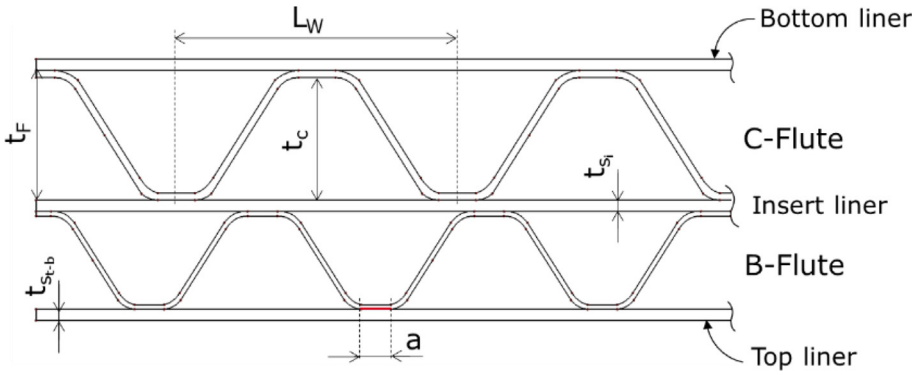

Fig. 2. Corrugated fiberboard geometry.

Table 1
Geometrical properties of BC fiberboard. All properties are given in mm.

Fiberboard components	Thickness t_s	Thickness t_F	Thickness t_C	Adhesion length a	Wavelength L_W
Top / Bottom liner	0.235				
Insert liner	0.153				
C-Flute		3.6	3.4125	1	7.2
B-Flute		2.5	2.375	0.8	6.1

Table 2
Corrugated fiberboard box properties.

Packaging dimensions	Length [mm]	Width [mm]	Height [mm]	Volume [L]	Mass [g]
Exterior	382	382	330		
Interior	368	368	302		
Outer packaging				40.9	831

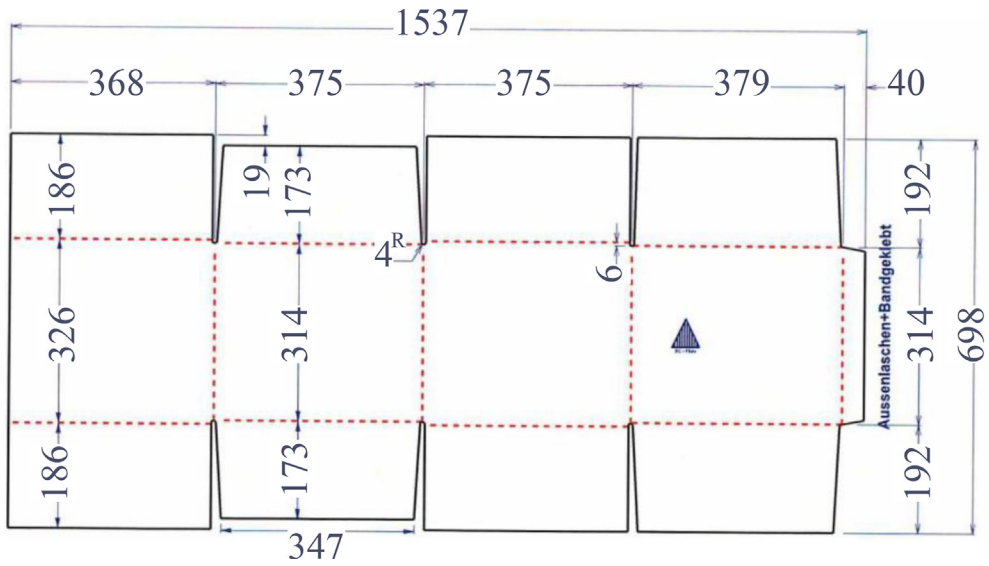

Fig. 3. Fiberboard box design according to FEFCO 0201 [11]. All dimensions are given in mm.

ducibility and reduce complexity of modeling. The combined mass of 4G packaging and substitute filling substance is 18 kg. The complete filled corrugated fiberboard box is shown in Fig. 4.

The box is sealed with a 75 mm wide cross-woven fiber-reinforced self-adhesive tape that has a tensile strength of 300 N/cm at a 10 % elongation at break. As seen in Fig. 4, the preferred regulation compliant closure type is a Double-T-Seal (closed 6-tape seal). This is necessary due to the nature of the small-grained filling substance which would otherwise spill out and require an interlayer between packaging and filling. Fig. 5 shows the 4G packaging brought to position for the drop test. The package is placed in a fixed position where the corner of the manufacturer's joint will be the first point of contact with the impact surface [6].

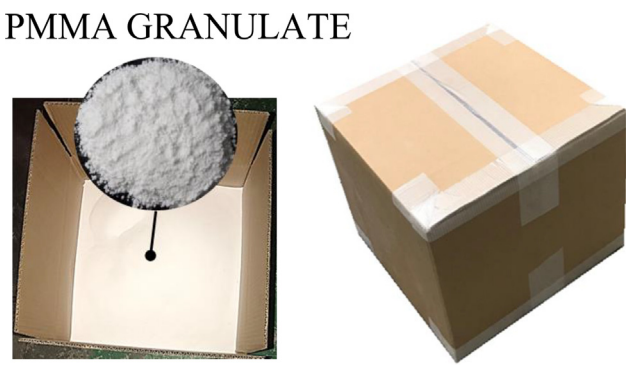

Fig. 4. Complete, filled fiberboard box.

The impact angle is controlled by an edged metal sheet angle with a steel rod attached to it. The metal sheet angle is applied on the inside of the box. This ensures drop position reproducibility. A device for moment-free dropping is used that is connected to the hook of an overhead crane. Preliminary tests were carried out to guarantee reproducibility and repeatability for impact position and impact angle with respect to the packaging's center of gravity.

2.2. Sensing equipment of the drop test

The packaging's and target's mechanical response to impact are captured by means of DIC which enables 3D deformation measurement and point tracking. Round target stickers applied on the impact target function as markers which are necessary to create a reference system for tracking local displacements. By means of a commercial digital photogrammetry system (GOM Correlate), numerous amounts of photos of different points of view are used to define a coordinate system with respect to the markers (see Fig. 6). This creates a plane corresponding to the impact surface according to the least squares method.

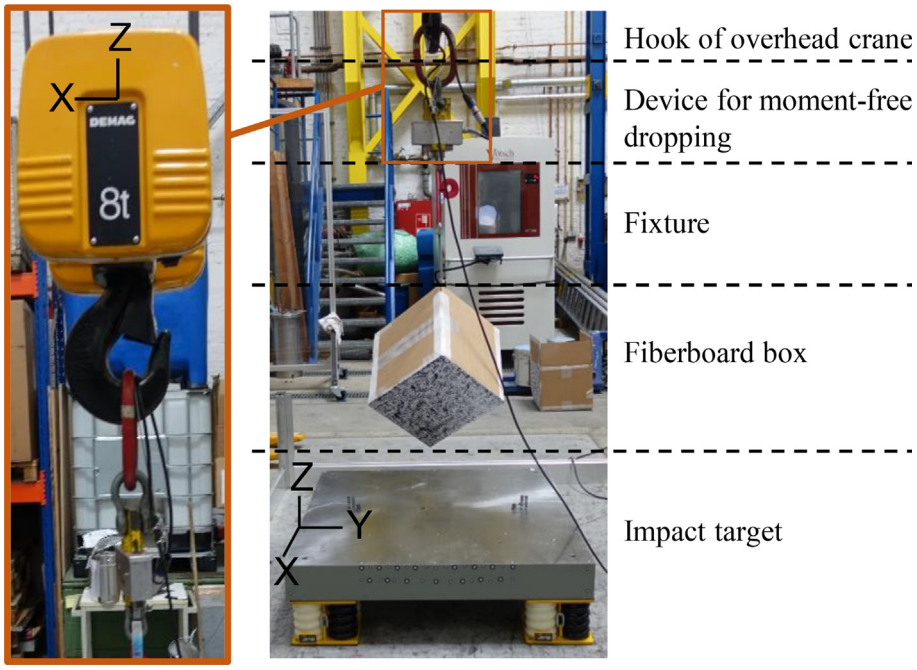

Fig. 5. Experimental drop test of the 4G packaging.

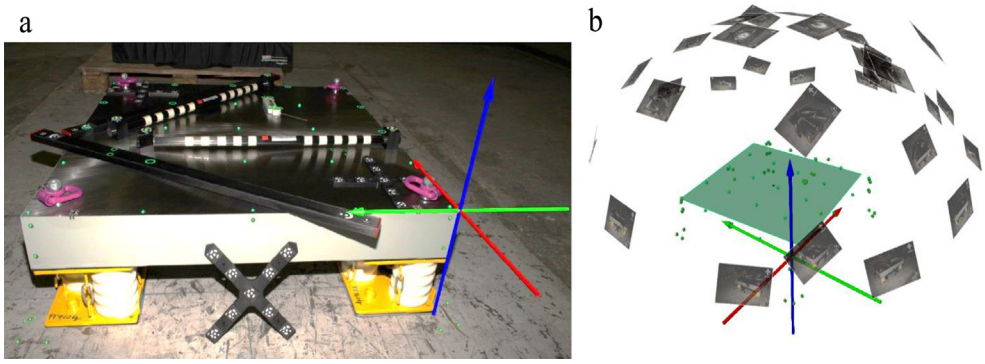

Fig. 6. (a) Impact target with calibration equipment and markers; (b) Digital reconstruction and reference system generation.

To capture the impact event of the drop test, two PHOTRON FASTCAM high-speed cameras are operated at a frame rate of 20 kHz and a resolution of 1024 × 1024 pixels. The setup is depicted in Fig. 7.

The side of the fiberboard box in the camera line of sight is painted white and provided with a random pattern of black spots, as shown in Fig. 8. This grayscale pattern is necessary for the generation of a high-quality digital 3D surface (consisting of a mesh of triangular elements) of the respective packaging side. This allows for the accurate computation of 3D displacements. Furthermore, the data noise is identified before each measurement in order to determine the measurement uncertainty. The range of data noise across all optical measurements was approximately ± 10 µm.

In addition to DIC, uniaxial IEPE accelerometers with an amplitude range of ± 50 g and a frequency range up to 10,000 Hz are applied on the impact surface. The response of the impact surface is captured and cross-referenced with the respective image correlation data. Thereby, the acceleration-time history is used to derive the relative displacements at the monitored locations by means of numerical integration. The expanded measurement uncertainty of the IEPE measurements was approximately ± 2 %.

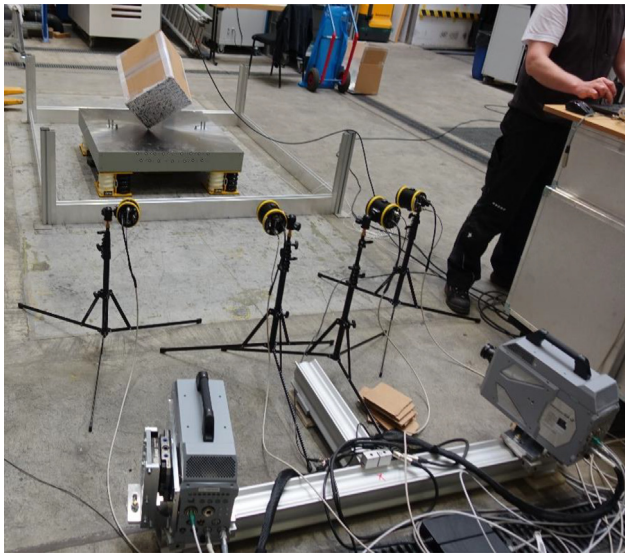

Fig. 7. Experimental setup with two PHOTRON FASTCAM high-speed cameras.

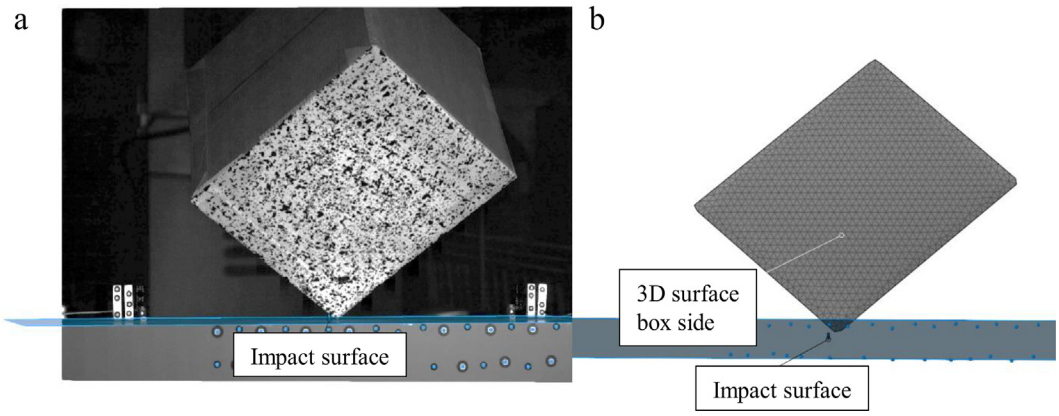

Fig. 8. (a) grayscale pattern on fiberboard box; (b) corresponding digital 3D surface.

2.3. Finite element structural modeling

The FE-model of the impact target consists of three parts: steel plate, springs, and ground. The steel plate is modeled with a fine homogeneous mesh of solid hexahedral elements. The spring elements are modeled as discrete one-dimensional elements defined by the spring constant in vertical direction. A rigid plate of solid elements with constrained translations and rotations in all directions is used for the ground. The model of the entire structure is shown in Fig. 9.

An implicit static analysis of gravity loading was carried out to investigate prestress of the steel plate. This is important for accurately simulating the mechanical response of the target structure during impact. Mass damping is also invoked and set at 10 % of critical damping to simulate vibration decay. The eigenfrequency of the system f_0 was derived analytically and experimentally in [4].

The modeling of the corrugated fiberboard and subsequently fiberboard box is realized through certain steps. An analytically homogenized fiberboard geometry, where the corrugated fiberboard properties are given by a mathematically equivalent homogeneous board geometry, as described in [12], was utilized to reduce computational times. This allows to define the same material properties through the thickness direction ZD. Thereby, the laminate theory for composite plates is used and enhanced by cal-

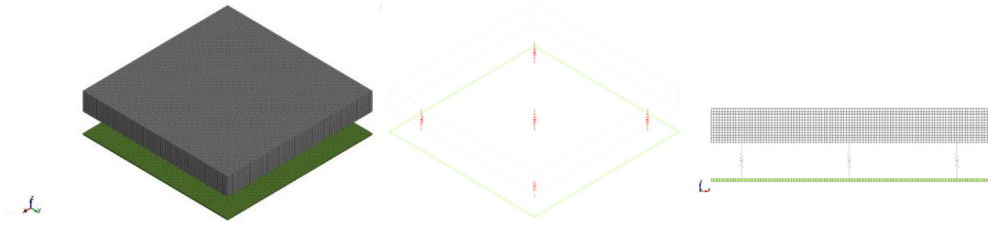

Fig. 9. FE model of impact target foundation structure.

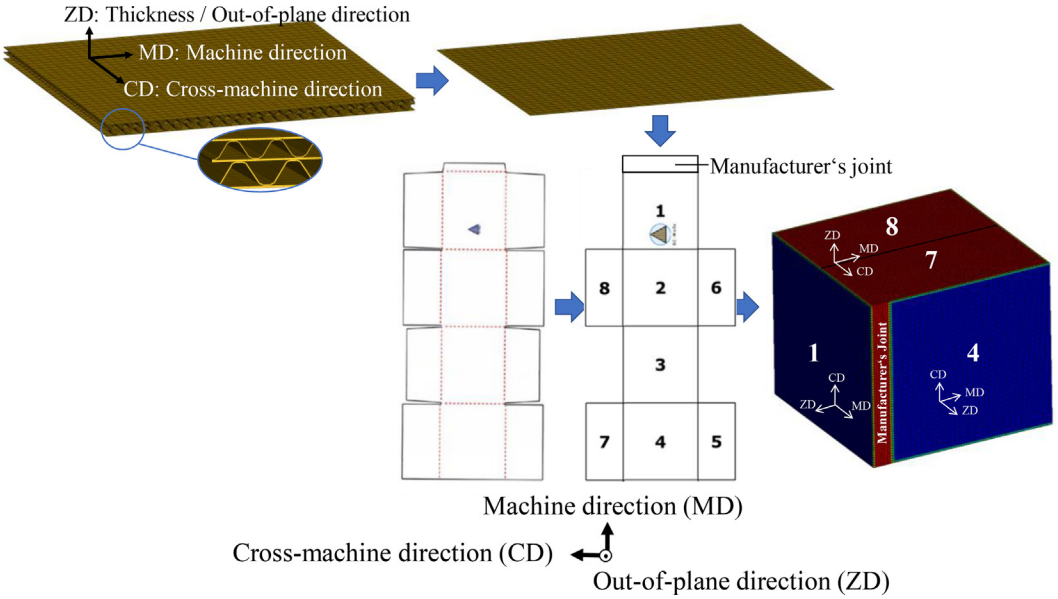

Fig. 10. FE-model generation of fiberboard box.

culating effective stiffnesses for the transverse shear and torsion moments. The finite-element mesh is modeled with fully integrated shell elements to achieve good results at high strain rates. Furthermore, the box geometry is simplified to achieve stability. The whole generation process of the finite-element model of the fiberboard box is described in Fig. 10.

As denoted in Fig. 10 by the red colored shell elements, the walls no. 5–8 and the manufacturer's joint are given double thicknesses to approximate the folding pattern. The fiber-reinforced tape is modeled as well, but only for the impact side (see Fig. 10; walls no. 5, 6) since loading of the opposite-side walls (no. 7, 8) is negligible. The Double-T-Seal closure is comprised of fully integrated shell elements with nodes that are tied to the respective faces on the box, as shown in Fig. 11. Therewith, the tape adheres ideally to the fiberboard.

The PMMA granulate filling substance is modeled in the simulations by means of the Smoothed-Particle-Hydrodynamics (SPH) method [13–15]. Thereby, the substance is approximated as a continuum by a set of homogeneously distributed particles around the packaging's center of mass. Each particle is assigned material coordinates which are independent variables. This particle based probabilistic method allows for large material distortion and fragmentation, as well as free surface flow. The model for the filling substance is visualized in Fig. 12.

The SPH particles enable fast computation times in explicit problems with fluid–structure interactions. This is important since the accurate representation of the interaction between filling substance and fiberboard box packaging is crucial for achieving a realistic deformation pattern in the transient impact simulation.

2.4. Material modeling

The fiberboard material is modeled by means of a preset in LS-DYNA [16] labeled as MAT_274 for paper and paperboard. This modeling approach is based on the work of Nygårds et al [17] and Xia et al [18]. Thereby, an elastoplastic model with decoupled in-plane and out-of-plane properties is used. The in-plane properties (plane spanned by MD and CD, see Fig. 10) are defined by orthotropic elasticity with six yield conditions (tension in MD, tension in CD, positive shear, compression in MD, compression in CD,

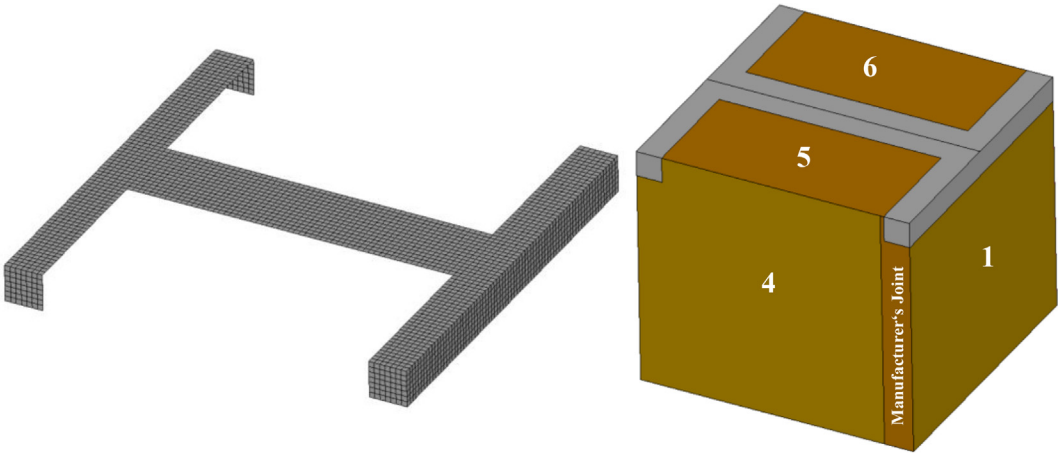

Fig. 11. FE-model of Double-T-Seal closure (on impact side).

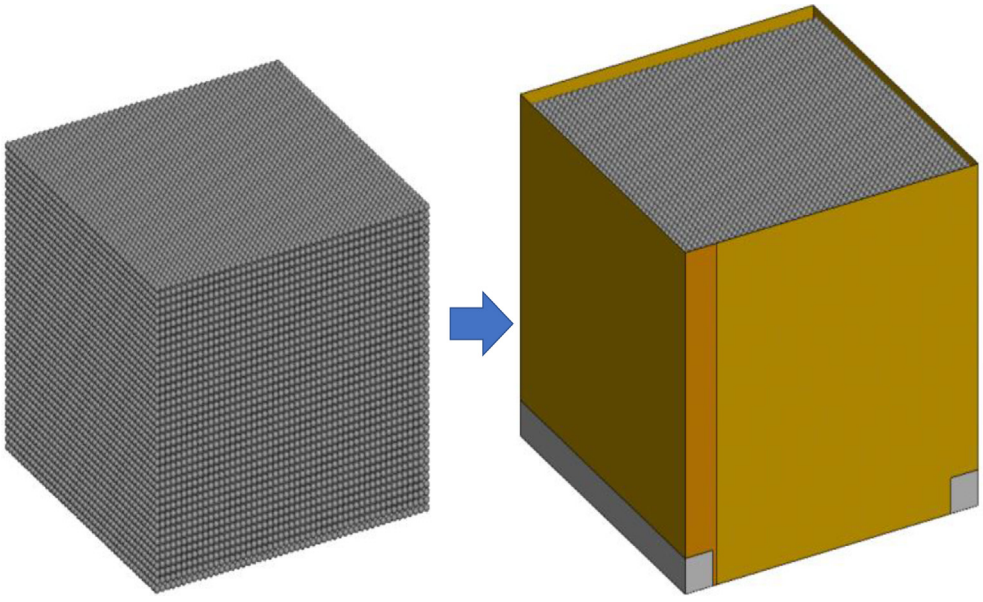

Fig. 12. Model of filling substance with SPH particles.

negative shear), each with their own independent hardening functions. The out-of-plane properties are described by empirical models which account for the non-linear elastic material behavior in compression in ZD, and the respective out-of-plane and transverse shear flow surfaces. The required elastic material constants were derived from tensile testing of fiberboard samples in MD and CD direction as well as calculations according to [19,20]. By means of curve-fitting of the hardening functions to the measured stress–strain curves, the plasticity parameters for tension in MD and CD were approximated. The remaining plasticity parameters were chosen in agreement with the literature [17,18,20]. Implementing the homogenization of the corrugated fiberboard geometry, the equivalent material parameters were calculated and are tabulated in Table 3.

To define the properties of the substitute filling substance, an equation of state (EOS) is defined. The bulk behavior of the material is determined by the EOS which calculates the pressure component of the total stress (hydrostatic behavior) as a function of density [21,22]. It is assumed that deviatoric stresses in bulk material behavior are negligible. In LS-DYNA, the material type card MAT_NULL allows equations of state to be considered without computing deviatoric stresses. An appropriate EOS to calculate the pressure component P is the polynomial form as described in Equation (1) [16]. Thereby, pressure is linear in internal Energy E and a function of μ, where $\mu = \rho/\rho_0 - 1$ with ρ being the current density and ρ_0 the reference density.

Table 3
Homogenized fiberboard material properties.

Material parameter	Value	Material parameter	Value
Density ρ [kg/m^3]	115	Hardening parameter $A_{0,3}$ [MPa]	6
E-modulus in MD E_1 [MPa]	283	Hardening parameter $B_{0,3}$ [-]	310
E-modulus in CD E_2 [MPa]	197	Hardening parameter $C_{0,3}$ [MPa]	225
E-modulus in ZD E_3 [MPa]	1.41	In-plane plasticity yield parameter $S_{0,4}$ [MPa]	7.3
Poisson's ratio ν_{21} [-]	0.25	Hardening parameter $A_{0,4}$ [MPa]	6
Poisson's ratio ν_{32} [-]	0.01	Hardening parameter $B_{0,4}$ [-]	160
Poisson's ratio ν_{31} [-]	0.01	Hardening parameter $C_{0,4}$ [MPa]	300
Shear modulus G_{12} [MPa]	91.4	In-plane plasticity yield parameter $S_{0,5}$ [MPa]	6.3
Shear modulus G_{23} [MPa]	5.64	Hardening parameter $A_{0,5}$ [MPa]	9
Shear modulus G_{13} [MPa]	5.14	Hardening parameter $B_{0,5}$ [-]	310
Elastic compression parameter E_3^c [-]	0.38	Hardening parameter $C_{0,5}$ [MPa]	225
Elastic compression exponent C_C [-]	16.3	Tensile plastic Poisson's ratio in MD ν_{1p} [-]	0.5
Exponent in in-plane yield surface T_{WOK} [-]	2	Tensile plastic Poisson's ratio in CD ν_{2p} [-]	0.13
In-plane plasticity yield parameter $S_{0,1}$ [MPa]	12	Compressive plastic Poisson's ratio in MD ν_{4p} [-]	0.5
Hardening parameter $A_{0,1}$ [MPa]	19	Compressive plastic Poisson's ratio in CD ν_{5p} [-]	0.13
Hardening parameter $B_{0,1}$ [-]	266	Out-of-plane plasticity yield parameter A_σ [MPa]	11.9
Hardening parameter $C_{0,1}$ [MPa]	800	Out-of-plane hardening parameter B_σ [MPa]	1.92
In-plane plasticity yield parameter $S_{0,2}$ [MPa]	6.5	Out-of-plane hardening parameter C_σ [MPa]	6
Hardening parameter $A_{0,2}$ [MPa]	40	Transverse shear plasticity yield parameter τ_0 [MPa]	0.95
Hardening parameter $B_{0,2}$ [-]	177	Transverse shear hardening parameter A_τ [MPa]	9
Hardening parameter $C_{0,2}$ [MPa]	250	Transverse shear hardening parameter B_τ [MPa]	2
In-plane plasticity yield parameter $S_{0,3}$ [MPa]	6		

$$P = C_0 + C_1\mu + C_2\mu^2 + C_3\mu^3 + (C_4 + C_5\mu + C_6\mu^2)E \quad (1)$$

In this case, the most important parameter to simulate bulk behavior is given by the polynomial coefficient C_1 which represents the elastic bulk modulus [21]. All other polynomial coefficients, i.e., C_0, C_2, C_3, C_4, C_5, and C_6 are set to zero. Thus, the pressure component of total stress is based only on volumetric strain. The respective values of the material properties are shown in Table 4.

An orthotropic elastic material model for the cross-woven fiber-reinforced adhesive tape is defined, according to manufacturer's specifications. Considering a plane spanned by two axes (1 and 2) which correspond to the directions of the length and width of a strip of tape, the respective young's moduli are defined as $E_1 = 1500$ MPa and $E_2 = 900$ MPa. Out-of-plane normal and shear stresses are negligible (plane stress behavior), since the thickness of the tape is very small compared to its other dimensions.

3. Results and discussion

The drop test was performed experimentally and simulated. There were 5 drop tests captured with DIC from a test series of 25 tests. The test series had the purpose of determining the drop height (i.e., the potential energy) from which a fiberboard box has a 50 % probability to fail the drop test [5]. From the 5 drop tests recorded by the high-speed cameras, one package failed the drop test. In total, 9 packages failed and had evident leakage of the filling substance. This helped greatly in identifying the activated failure mechanisms which are accurately represented in the simulation results. The drop test parameters are explicitly described in Table 5.

3.1. Validation of FE model

In Fig. 13, the 3D deformation measurement is compared with the simulation results. The contour plots display the relative displacements of the deformed state to the undeformed state in Y-direction with respect to a common coordinate system. The depicted timestamps are chosen to be representative of the increase of deformation until reaching maximum rigid body deflec-

Table 4
PMMA granulate material properties.

Material parameter	Value
Density ρ_0 [kg/m^3]	460
1st polynomial equation coefficient (elastic bulk modulus) C_1 [MPa]	2000

Table 5
Drop test parameters.

Test parameters	
Packaging total weight [kg]	18
Drop height [m]	5.0 – 7.1
Drop position (ISO 2206 [6])	On a corner (Top corner/manufacturer's joint)
Impact target	Steel plate on bedding of high strength spring elements
Impact surface area [m^2]	1
Impact target mass [kg]	960
Total spring stiffness [kN/mm]	12.1
Point of impact	Centre of impact surface of target
Observed impact duration [ms]	50

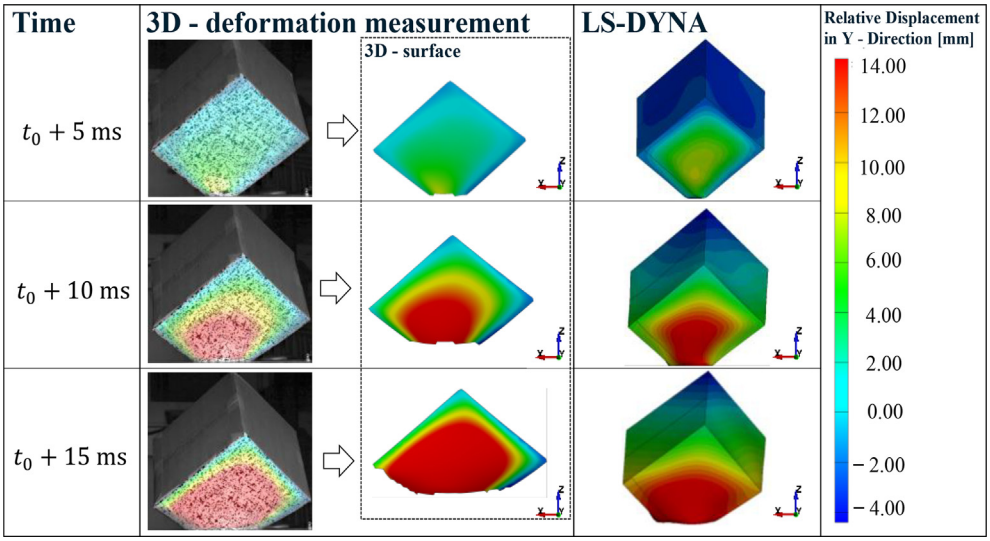

Fig. 13. Deformation comparison of fiberboard box side between optical 3D measurement and simulation.

tion and bulging of the observed side respectively. This occurs at approximately 15 ms after initial contact t_0 between the corner of the fiberboard box and the impact surface.

Furthermore, the rigid body deflection of packaging and target during impact are evaluated, as shown in Fig. 14. Firstly, a point with negligible relative displacement to the undeformed state is defined on the fiberboard box side and projected along the vertical axis onto the impact surface plane with respect to the defined reference system. This allows for tracking the distance between these two points which can be interpreted as the rigid body deflection of the package. Secondly, the impact target vibration is derived from the points defined in the photogrammetry procedure. Due to the considerably high mass of the target, the vibration data exhibit very small deviations across all considered points. The target behaves like a rigid body, and the elastic deformation of the impact surface is negligible. This is also backed up by impact simulations of the drop test as well as vibration analysis [4]. In this instance, the chosen position (Position 2, see Fig. 14) has the purpose of cross-referencing image, accelerometer, and simulation data. Thus, a round target sticker was applied directly onto the IEPE accelerometer for point tracking.

The result comparison shows very good agreement between experiments and FE simulation. This is illustrated by the graphs in Fig. 15 where the rigid body deflection is plotted against time for target and fiberboard box respectively, starting from the first moment of contact between the two objects.

3.2. Deformation and failure mechanisms of the filled fiberboard box

Two mechanisms which are activated on impact show significant influence on packaging deformation. On the one hand, there is bulging of the walls and on the other hand, there is creasing

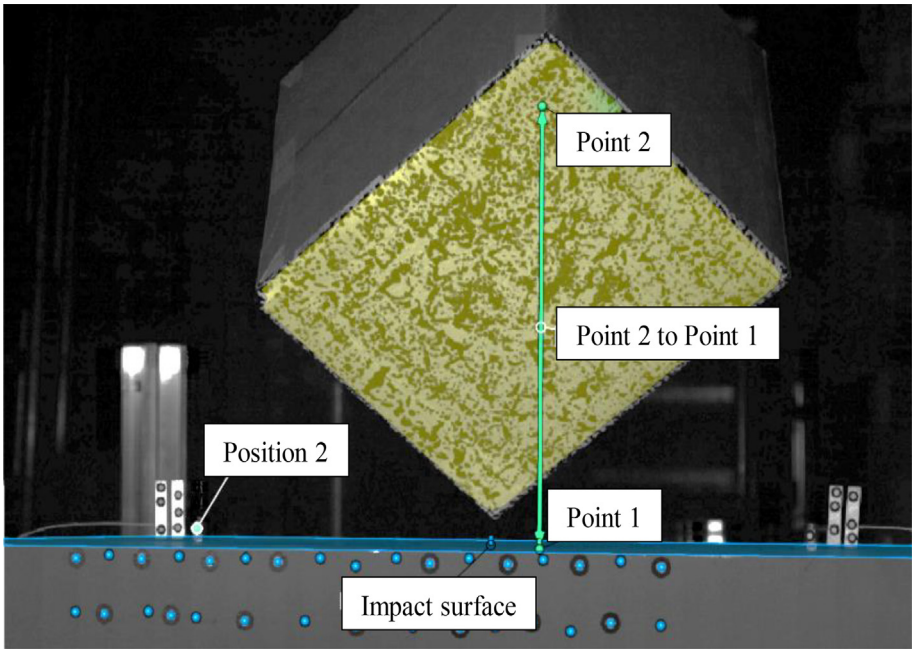

Fig. 14. Definition of measurement for rigid body deflection of fiberboard box and impact surface.

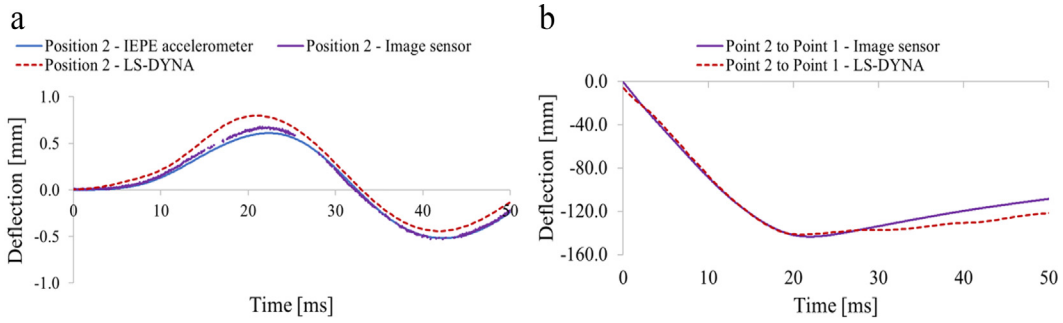

Fig. 15. (a) Rigid body deflection of impact surface; (b) Rigid body deflection of filled fiberboard box.

relating to delamination. The relevance of these effects is further supported by evidence found in [23–25].

Wall bulging occurs due to in-plane tension (see Fig. 16). Thereby, the extent of bulging is highly dependent on the inertia and bulk behavior of the filling substance. In addition, large bulging of the walls causes the edges of the box as well as the fiber-reinforced tape (joining walls no 5 and 6) to carry a significant amount of impact load.

The failure types that were observed experimentally correspond with this identified mechanism in the FE simulation, i.e., failure occurs at the critical moment $t_{crit} = t_0 + 15 \pm 2$ms of maximum deformation due to in-plane tension. On 5 instances of packaging

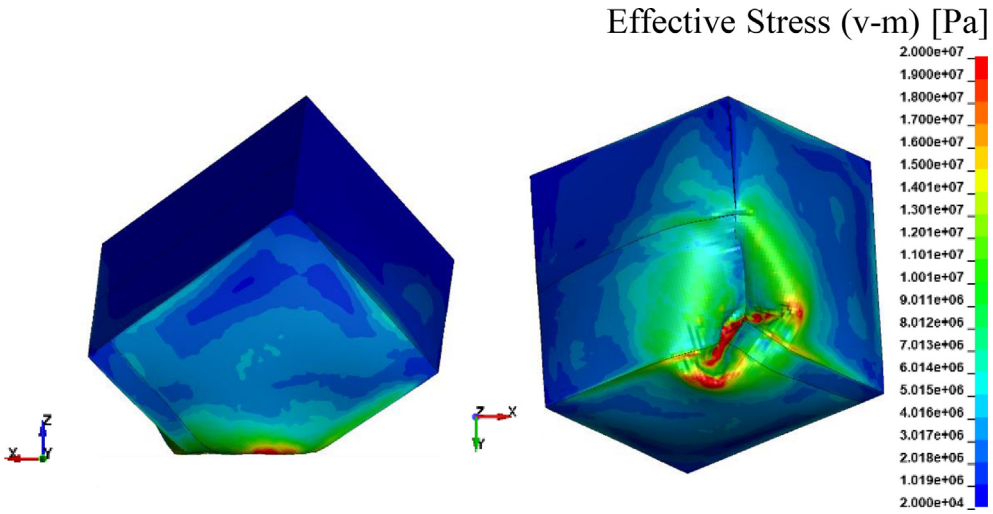

Fig. 16. Effects of in-plane tension response of the filled fiberboard box in corner drop test.

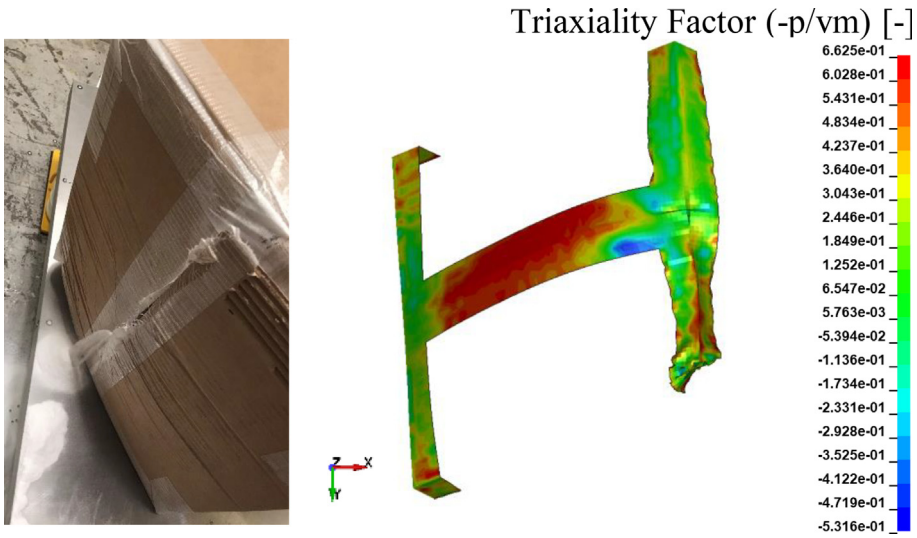

Fig. 17. Flexure-induced fracturing of fiber-reinforced tape-laminate.

failure out of a total of 9, there was flexure-induced fracturing of the tape-laminate, as illustrated in Fig. 17. This is attributed to the extensive loading of the tape which can be seen in the simulation results by the triaxiality factor (ratio of pressure forces to shear forces) contour plot. The triaxiality factor provides an interpretation of activation of failure mechanisms regarding fracture processes due to void extension, such as the tape-laminate fracturing due to the bulging of the coalesced walls no. 5 and 6. Hence, it is evident, that the tape quality used to seal fiberboard box packagings is crucial with regard to mechanical safety.

In the remaining 4 instances, there was distinct fracturing along the edge of the manufacturer's joint, as shown in Fig. 18. This is caused predominantly by tension forces and is the direct effect of large edge loading. However, a very high amount of impact energy is necessary to initiate this type of failure in the fiberboard material in a corner drop test (approx. more than 1200 Nm).

The second distinct type of deformation mechanism is described by high local strains due to in-plane compression and out-of-plane shear, e.g., caused by the substantial relative displacement of the box's corner (point of impact) which initiates local damage in form of creasing associated with delamination; see Fig. 19. This effect alone, however, did not lead to failure of the filled fiberboard box.

Regarding drop testing, crease formation contributes to the damping of impact energy and temporary reduction of the effective stress in the fiberboard box.

4. Conclusion

A validated finite-element simulation model for complete, filled fiberboard boxes was proposed based on experimental drop test results using highly accurate measuring techniques like digital image correlation. This approach enabled the identification of dominant deformation and failure mechanisms in filled fiberboard boxes in the context of mechanical safety testing of dangerous goods packagings. Thereby, creasing associated with delamination

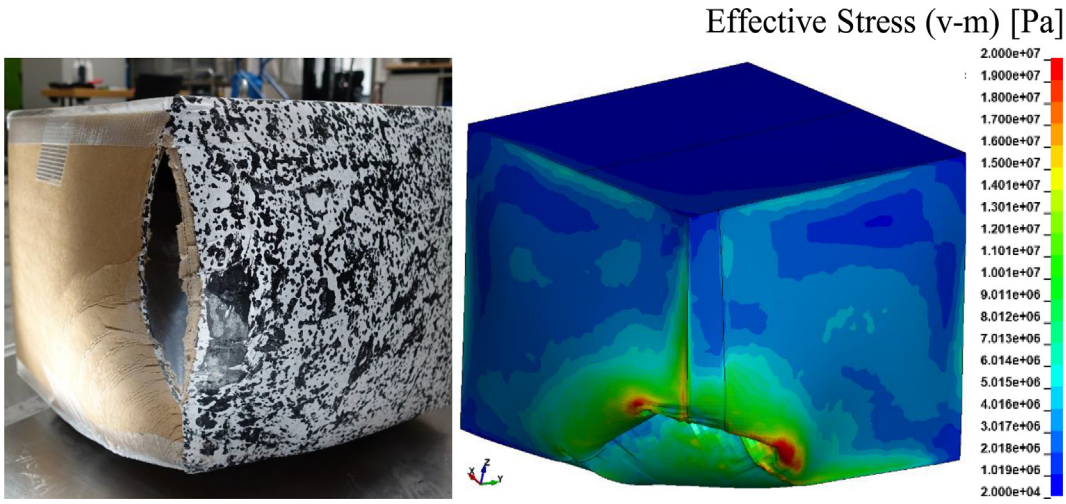

Fig. 18. Fracturing along the edge of the manufacturer's joint.

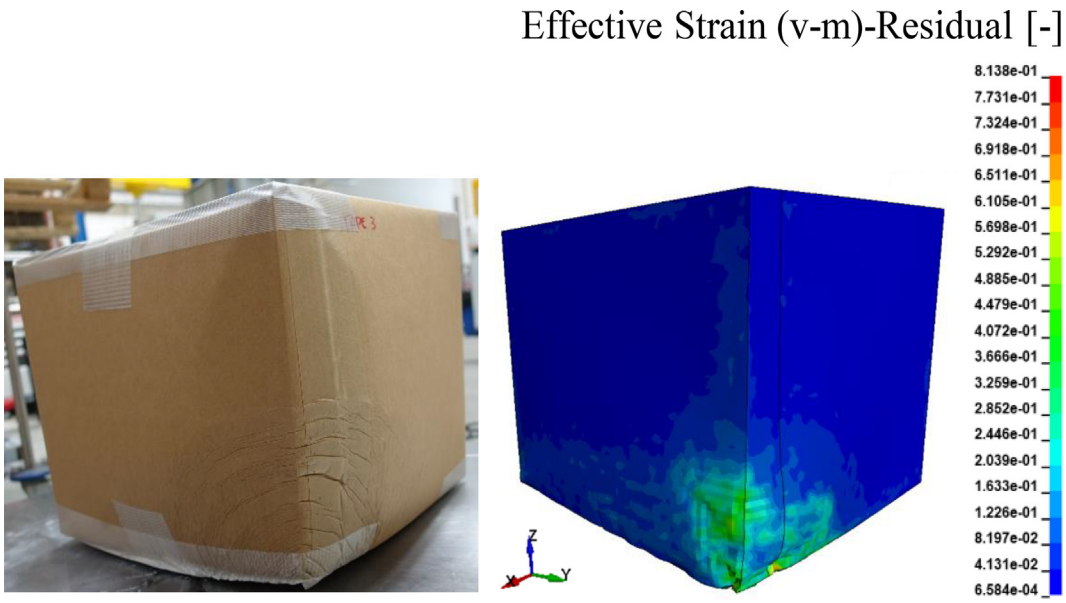

Fig. 19. Effects of in-plane compression and out-of-plane shear response of the filled fiberboard box in corner drop test.

and bulging of the fiberboard walls were major sources of deformation with the latter being responsible for initiating damage. The damage assessment highlights the importance of the properties of the adhesive tape used for sealing the package. The likelihood of failure for fiberboard boxes rises significantly with decreasing quality of tape-laminate. The findings of this work are highly relevant for industrial application. Using the described methods, parametrization of geometrical properties, board composition and material properties is possible to derive accurate models of manufacturer specific designs. Namely, modeling can be tailored to the needs of the respective manufacturer for achieving production of optimized regulation-compliant packaging.

CRediT authorship contribution statement

Nikolaos Lengas: Conceptualization, Methodology, Investigation, Software, Writing – original draft, Visualization. **Sergej Johann:** Investigation, Resources. **Daniel Kadoke:** Formal analysis, Software, Resources, Validation. **Karsten Müller:** Data curation, Supervision. **Eva Schlick-Hasper:** Project administration. **Marcel Neitsch:** Project administration. **Manfred W. Zehn:** Supervision.

Declaration of Competing Interest

The authors declare that they have no known competing financial interests or personal relationships that could have appeared to influence the work reported in this paper.

Data availability

Data will be made available on request.

Acknowledgment

This work is part of a research project funded internally by BAM Federal Institute for Materials Research and Testing.

References

[1] UN Recommendations on the Transport of Dangerous Goods - Model Regulations. Twenty-first revised edition, United Nations, 2019. https://unece.org/rev-21-2019
[2] Agreement concerning the International Carriage of Dangerous Goods by Road (ADR), applicable as from 1. January 2021. https://unece.org/transport/documents/2021/01/standards/adr-2021-volume-1.
[3] ISO 2248: 1985-12. Packaging – Complete, filled transport packages – Vertical impact test by dropping. International Organization for Standardization
[4] N. Lengas, K. Müller, E. Schlick-Hasper, M. Neitsch, S. Johann, M.W. Zehn, Development of an analysis and testing concept for the evaluation of impact targets in the mechanical safety testing of dangerous goods packagings, Packag. Technol. Sci. 35 (9) (2022) 689–700, https://doi.org/10.1002/pts.2656.
[5] Hück M. Ein verbessertes Verfahren für die Auswertung von Treppenstufenversuchen. In: Materialwissenschaft und Werkstofftechnik 14; 1983, Nr. 12; p. 406–417. https://doi.org/10.1002/mawe.19830141207
[6] ISO 2206: 1987. Packaging – Complete, filled transport packages – Identification of parts when testing. International Organization for Standardization
[7] Hopmann C, Klein J. Determination of strain rate dependent material data for FEA crash simulation of polymers using digital image correlation. Comput. Mater. Sci. Volume 100, Part B. 2015; p. 181–190. https://doi.org/10.1016/j.commatsci.2015.01.021
[8] B. Pan, W. Dafang, X. Yong, Incremental calculation for large deformation mesurement using reliability-guided digital image correlation, Opt. Lasers Eng. 50 (4) (2012) 586–592, https://doi.org/10.1016/j.optlaseng.2011.05.005.
[9] Holmes J, Sommacal S, Das R, Stachurski Z, Compston P. Digital image and volume correlation for deformation and damage characterisation of fibre-reinforced composites: A review. Compos. Struct. Volume 315. 2023. 116994. https://doi.org/10.1016/j.compstruct.2023.116994.
[10] ISO 3034: 2011. Corrugated fibreboard – Determination of single sheet thickness. International Organization for Standardization
[11] FEFCO code. Design style library for corrugated board products. 12th ed. 2022. www.fefco.org.
[12] Talbi N, Batti A, Ayad R, Guo Y.Q. An analytical homogenization model for finite element modelling of corrugated cardboard. Composite Structures. Volume 88, Issue 2. 2009; p. 280–289. https://doi.org/10.1016/j.compstruct.2008.04.008.
[13] R. Hedayati, S. Ziaei-Rad, Effect of bird geometry and orientation on bird-target impact analysis using SPH method, Int. J. Crashworthiness 17 (4) (2012) 445–459, https://doi.org/10.1080/13588265.2012.674333.
[14] Jackson KE, Fuchs YT. Comparison of ALE and SPH Simulations of Vertical Drop Tests of a Composite Fuselage Section into Water. 10th International LS-DYNA User's Conference. 2013. https://ntrs.nasa.gov/api/citations/20080022946/downloads/20080022946.pdf.
[15] A. Rafiee, M.T. Manzari, M. Hosseini, An incompressible SPH method for simulation of unsteady viscoelastic free-surface flows, Int. J. Non Linear Mech. 42 (10) (2007) 1210–1223, https://doi.org/10.1016/j.ijnonlinmec.2007.09.006.
[16] LS-DYNA Keyword User's Manual. Volume II Material Models, Livermore Software Technology (LST), An ANSYS Company. 2021
[17] M. Nygårds, M. Just, J. Tryding, Experimental and numerical studies of creasing of paperboard, Int. J. Sol. Struct. 46 (2009) 2493–2505, https://doi.org/10.1016/j.ijsolstr.2009.02.014.
[18] Q. Xia, M. Boyce, D. Parks, A Constitutive model for the anisotropic elastic-plastic deformation of paper and paperboard, Int. J. Sol. Struct. 39 (2002) 4053–4071, https://doi.org/10.1016/S0020-7683(02)00238-X.
[19] ISO 1924 – 3: 2005. Paper and board – Determination of tensile properties – Part 3: Constant rate of elongation method (100 mm/min). International Organization for Standardization
[20] P. Mäkelä, S. Östlund, Orthotropic elastic–plastic material model for paper materials, Int. J. Sol. Struct. 40 (2003) 5599–5620, https://doi.org/10.1016/S0020-7683(03)00318-4.
[21] D. Grady, Equation of state for solids, AIP Conf. Proc. 1426 (800) (2012) 800–803, https://doi.org/10.1063/1.3686399.
[22] Laine L, Sandvik A. Derivation of mechanical properties for sand. Proceedings of the 4th Asia-Pacific Conference on Shock and impact loads on structures, CI-Premier PTE LTD, Singapore. Volume 361. ANSYS Inc., 2001; p. 361–368.
[23] M. Nygårds, S. Sjökvist, G. Marin, J. Sundström, Simulation and experimental verification of a drop test and compression test of a gable top package, Packag. Technol. Sci. 34 (4) (2021) 229–243, https://doi.org/10.1002/pts.2441.
[24] Gong G, Liu Y, Fan B, Sun D. Deformation and compressive strength of corrugated cartons under different indentation shapes: Experimental and simulation study. Packag Technol Sci. Volume 33, Issue 6; p. 215–226. https://doi.org/10.1002/pts.2499.
[25] Luong VD, Abbès F, Abbès B, Minh Duong PT, Nolot JB, Erre D, Guo YQ. Finite Element Simulation of the Strength of Corrugated Board Boxes Under Impact Dynamics. Proceedings of the International Conference on Advances in Computational Mechanics 2017. ACOME 2017; p.369–380. https://doi.org/10.1007/978-981-10-7149-2_25